

ENHANCING BIOGENIC EMISSION MAPS USING DEEP LEARNING

Antonio Giganti, Sara Mandelli, Paolo Bestagini, Marco Marcon, Stefano Tubaro

Dipartimento di Elettronica, Informazione e Bioingegneria - Politecnico di Milano - Milan, Italy

ABSTRACT

Biogenic Volatile Organic Compounds (BVOCs) play a critical role in biosphere-atmosphere interactions, being a key factor in the physical and chemical properties of the atmosphere and climate. Acquiring large and fine-grained BVOC emission maps is expensive and time-consuming, so most of the available BVOC data are obtained on a loose and sparse sampling grid or on small regions. However, high-resolution BVOC data are desirable in many applications, such as air quality, atmospheric chemistry, and climate monitoring. In this work, we propose to investigate the possibility of enhancing BVOC acquisitions, taking a step forward in explaining the relationships between plants and these compounds. We do so by comparing the performances of several state-of-the-art neural networks proposed for Single-Image Super-Resolution (SISR), showing how to adapt them to correctly handle emission data through preprocessing. Moreover, we also consider realistic scenarios, considering both temporal and geographical constraints. Finally, we present possible future developments in terms of Super-Resolution (SR) generalization, considering the scale-invariance property and super-resolving emissions from unseen compounds.

Index Terms— BVOC, Biogenic Emissions, Isoprene, SISR, Super-Resolution

1. INTRODUCTION

Terrestrial ecosystems generate many chemicals, including volatile and semi-volatile compounds released into the atmosphere. Some of them, such as Biogenic Volatile Organic Compounds (BVOCs), play critical roles in atmospheric chemistry [1]–[3]. Their oxidation in the atmosphere affects tropospheric photochemistry and composition [4]. BVOC's oxidation products promote the formation of low-level ozone and secondary organic aerosols, thus having a huge impact on air quality and earth's radiative budget [5], [6].

For these reasons, quantitative estimations of BVOC emissions are required for numerical evaluations of past, current, and future air quality and climate conditions [1], [2], [7]. BVOC emissions are now routinely included in coupled climate and chemistry models such as regional and global air quality and earth system models [8]. Different ground-based measurement techniques can be applied to sample BVOC emissions at diverse scales, from leaf to regional and global level [6], [7]. However, available measurements are limited in space and time, therefore they might be not fully suitable to perform reliable simulations of atmospheric, climate, and forecasting models.

We propose to overcome this problem by generating a more dense spatial grid of BVOC emissions, starting from a coarser one. We formulate the problem as a Single-Image Super-Resolution (SISR) task, a general problem of computationally enhancing the

This work was supported by the Italian Ministry of University and Research (MUR) and the European Union (EU) under the PON/REACT project.

resolution of a digital image. The problem is ill-posed since multiple different High Resolution (HR) images are consistent with a single Low Resolution (LR) image. Therefore, the task of Super-Resolution (SR) is to constrain the problem to find a unique mapping between a LR image and its HR counterpart in such a way that the LR image is upscaled with high fidelity.

Several SR approaches have been proposed in the literature. Before the Deep Learning (DL) era, “classical” methods were based on different working principles (e.g., sparse neighbor embedding [9], edge sharpening [10], etc.). Starting with the seminal work of the Super-Resolution Convolutional Neural Network (SRCNN) [11], methods based on DL are nowadays widely studied for the problem of SR, proving superior to classical methods. A detailed review of deep learning for SR can be found in [12].

Applying SR techniques to BVOC emission maps is not straightforward. Indeed many works on SISR focus on enhancing images that are evaluated by visual inspection (e.g., photographs, biomedical data, etc.). However, BVOC data have different characteristics than photographs. BVOC are physical measures linked to a meaningful measurement unit (e.g., we cannot observe negative emissions). Moreover, BVOC dynamic range is strongly different compared to classic 8-bit imagery. It is, therefore, necessary to study a way of adapting SISR techniques to this kind of data.

Dealing with data different from natural images is a well-known issue for researchers who apply SR algorithms to enhance the quality and utility of satellite data [13]. For example, the authors of [14] improved the resolution of Land Surface Temperature (LST) data using a U-Net-based architecture. Recently, SR of Sea Surface Temperature (SST) has been addressed in [15] and in [16]. In the latter work, the authors exploited the different correlations between optical and thermal images to improve the accuracy of the super-resolved SST data. The improvement of trajectory calculations of wind fields for enhancing the reliability of particle dispersion model for meteorological purposes was addressed in [17], where authors implement an attention mechanism to increase the performance in SR.

To the best of our knowledge, there are no studies for super-resolving BVOC emission maps. The proposed study can provide dense data for the atmospheric chemical, climate, and air quality models. In addition, upsampling biogenic emission maps can be helpful for a variety of tasks, e.g., to capture small-scale processes, to improve characterization of the complex interaction between BVOCs and other chemical compounds, and to better quantify emissions induced from abiotic [18]–[20] and ozone stress [5], [21].

In this work, we explore the potential of deep learning to enhance the resolution of BVOC emission maps. We do so by investigating seven state-of-the-art neural network architectures for SISR, training them with emission maps taken from a recent high-resolution biogenic global emission inventory [4]. The proposed method enables the synthesis of emission maps making a significant step toward fulfilling the wishes of atmospheric chemical and climate modeling communities.

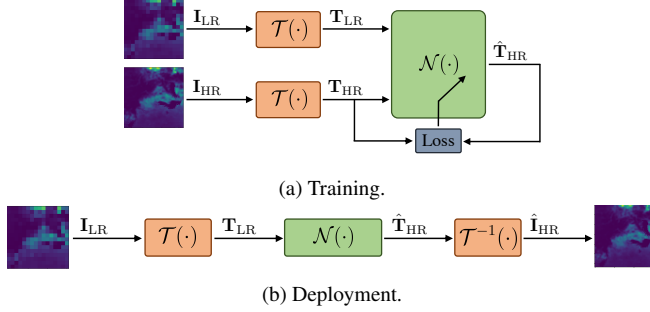


Fig. 1: The proposed method: (a) training and (b) deployment phase.

2. BVOC SUPER RESOLUTION

In this work, we consider the problem of recovering a high-resolution BVOC emission map \mathbf{I}_{HR} from a low-resolution emission map \mathbf{I}_{LR} , which can be seen as a SISR task. Fig. 1 shows a sketch of the proposed methodology. We estimate a super-resolved emission $\hat{\mathbf{I}}_{\text{HR}}$ by starting from the low-resolution emission \mathbf{I}_{LR} as

$$\hat{\mathbf{I}}_{\text{HR}} = \mathcal{T}^{-1}(\mathcal{N}(\mathcal{T}(\mathbf{I}_{\text{LR}}))),$$

where $\mathcal{T}(\cdot)$ is a transformation applied to the low-resolution emission, $\mathcal{N}(\cdot)$ is the operator applied by a neural network, and $\mathcal{T}^{-1}(\cdot)$ is the inverse transformation of $\mathcal{T}(\cdot)$. In our work, we model \mathbf{I}_{LR} as a matrix with size $M \times N$. \mathbf{I}_{HR} and its estimation $\hat{\mathbf{I}}_{\text{HR}}$ have size $\alpha M \times \alpha N$, with $\alpha > 1$ indicating the super-resolution factor (i.e., how much we increase the resolution).

The network training phase involves $(\mathbf{I}_{\text{LR}}, \mathbf{I}_{\text{HR}})$ emission pairs as input (see Fig. 1a). We consider the Mean Squared Error (MSE) between the transformed emissions as a loss function. At testing stage (see Fig. 1b), given an \mathbf{I}_{LR} emission to be super-resolved, we estimate $\hat{\mathbf{I}}_{\text{HR}}$ from the network. Then, we return to the original emission's range by applying the inverse data transformation \mathcal{T}^{-1} , obtaining the super-resolved emission $\hat{\mathbf{I}}_{\text{HR}}$.

2.1. Data Transformation

BVOC emissions are spatially sparse, reporting extremely small values and a wide dynamic range (from 10^{-30} to 10^{-9} [kg/m²s] [4]). Transforming this dynamics into more feasible values is crucial for numerical stability when training the network. To obtain emission maps with a dynamic range in $[0, 1]$, we investigate two data transformation strategies, obtaining $\mathbf{T}_{\text{LR}} = \mathcal{T}(\mathbf{I}_{\text{LR}})$ and $\mathbf{T}_{\text{HR}} = \mathcal{T}(\mathbf{I}_{\text{HR}})$, respectively:

- \mathcal{T}_{S} — *Emission Scaling*: the preprocessed emissions are obtained by dividing \mathbf{I}_{LR} and \mathbf{I}_{HR} by their maximum, i.e., $\mathbf{T}_{\text{LR}} = \mathbf{I}_{\text{LR}}/\mathbf{I}_{\text{LR},\text{max}}$, $\mathbf{T}_{\text{HR}} = \mathbf{I}_{\text{HR}}/\mathbf{I}_{\text{HR},\text{max}}$;
- \mathcal{T}_{Q} — *Quantile Transformation*: \mathbf{T}_{LR} and \mathbf{T}_{HR} are obtained by re-mapping \mathbf{I}_{LR} and \mathbf{I}_{HR} with a non-parametric transformation into a uniform distribution with values between 0 and 1 [22]. \mathcal{T}_{Q} can be seen as an invertible histogram equalization procedure aiming at linearizing the Cumulative Distribution Function (CDF) of the data. This transformation must be learnt from some reference data to map the dynamic range of a generic input uniformly in $[0, 1]$. We propose to learn the transformation directly from the HR emissions during the training phase.

It has been proven that \mathcal{T}_{Q} preprocessing is less influenced by outliers than \mathcal{T}_{S} preprocessing [22]. This property is beneficial in the context of BVOC emissions because there can be many outliers due

to the large spatial diversity of the environmental factors driving the emission process, such as meteorology, type of vegetation, seasonal cycle, and atmospheric composition [4].

Another difference between the two preprocessing is related to retrieving information regarding the maximum peak emission. Indeed, due to the inherent low resolution of LR maps, it is common to miss out the maximum emission value of HR maps in their related LR version. In other words, it may happen very often that $\mathbf{I}_{\text{LR},\text{max}} < \mathbf{I}_{\text{HR},\text{max}}$, for each $(\mathbf{I}_{\text{LR}}, \mathbf{I}_{\text{HR}})$ pair. If this happens, \mathcal{T}_{S} scaling provides us with a processed version of \mathbf{I}_{LR} that is not consistent with the distribution of data in \mathbf{I}_{HR} . On the contrary, \mathcal{T}_{Q} preprocessing performs a non-linear transformation based on *a priori* information extracted from statistical analysis of the HR data. This is not sensitive to single outlier or local maxima values in the data, making the distribution of \mathbf{I}_{LR} and \mathbf{I}_{HR} transformed data compatible.

2.2. SR Networks

We compare 7 different state-of-the-art neural networks for SISR, investigating the adoption of different configurations and learning paradigms. The investigated networks are the following:

- SRCNN [11], which is a pioneer work based on Convolutional Neural Networks (CNNs).
- Super-Resolution Generative Adversarial Network (SRGAN) [23], where the authors define a novel perceptual loss based on feature maps of the Visual Geometry Group (VGG) network.
- Residual Channel Attention Network (RCAN) [24], which is an attention-based framework. The recursive residual design allows multiple pathways for information flow from initial to final layers, and the selective attention allows to focus on specific feature maps that are more important for the end task.
- Enhanced SRGAN (ESRGAN) [25], which is an improved version of SRGAN including a different architecture for both the generator and the discriminator.
- Residual-in-Residual Dense Block Network (RRDBNet) [25], which combines complex multi-level residual network and dense connections.
- Second-order Channel Attention Network (SANSISR) [26], based on attention like RCAN. With respect to RCAN, a Second-order Attention Network (SAN) is proposed for more powerful feature correlation learning, using second-order feature statistics. The authors propose an additional block to capture long-distance spatial information and to exploit LR information, easing the training and bypassing low-frequency characteristics.
- Modified SRRResNet (MSRResNet) [27], which is a modified version of the original Super-Resolution ResNet (SRRResNet) [23], exploiting the benefits of the residual learning framework.

3. EXPERIMENTAL SETUP

3.1. Dataset

Inventories of real measurement of BVOC emissions are scarce and limited in time and space. However, the knowledge obtained from observations on the emission processes gives the possibility to simulate them for a specific temporal and spatial domain based on defined input parameters. We use the most recent global coverage biogenic emission inventory calculated by an emission model and presented in [4]. The inventory includes emissions from several biogenic compounds, covering the entire Earth surface in the period of 2000-2020, with a $0.25^\circ \times 0.25^\circ$ spatial resolution (i.e., $\approx 28\text{km} \times 28\text{km}$ of

the planet surface for each cell in continental regions). As far as we know, this is the most up-to-date global coverage biogenic emission inventory with the highest spatial resolution available in the literature. Emissions are reported as hour profiles and are averaged monthly.

Among the different biogenic compounds that are present in the inventory, we select isoprene since it is by far the most important in terms of both global emission and atmospheric impact [6], having an annual emission of about half of the total BVOCs emissions [5].

Each emission map has a grid of 1440×720 cells. We slice them to obtain smaller non-overlapped patches of size 64×64 cells. This makes the training more computationally manageable and allow us to assume that there are not many radial distortions due to the Earth curvature in the area. Since these maps are spatially sparse, a considerable amount contains zero emissions. Thus, we discard the patches with non-zero emissions below the 5%, avoiding unnecessary computation on zero-emission areas. We end up with 81957 different HR patches \mathbf{I}_{HR} that can be considered as ground truth. We generate the associated LR patches by performing bicubic down-sampling, obtaining the \mathbf{I}_{LR} emission maps of 16×16 cells. The $(\mathbf{I}_{\text{LR}}, \mathbf{I}_{\text{HR}})$ pairs constitute our final dataset $\mathcal{D} = \{\mathbf{I}_{\text{HR}i}, \mathbf{I}_{\text{LR}i}\}$, for $i = 1, \dots, 81957$. We aim at super-resolving LR emission maps, which have a $1^\circ \times 1^\circ$ spatial resolution, into HR emission maps with $0.25^\circ \times 0.25^\circ$ resolution, thus with scale factor $\alpha = 4$.

3.2. Training Setting

The transformation \mathcal{T}_Q requires the estimation of the quantiles used for mapping an emission probability distribution to the uniform one [22]. We train the algorithm exploiting all HR training data, with 1000 quantiles. Then, we preprocess \mathbf{I}_{HR} and \mathbf{I}_{LR} emissions with the estimated transformation. We keep this transformation fixed for what concerns further network training and deployment stages.

To train the networks, we divide our dataset into train, validation, and test sets with 70/20/10 percentage amount, respectively. We combine the ADAM optimizer with the Cosine Annealing (with restarts) learning rate scheduler [28], which enables to obtain faster computations and better results [29]. We use 50k iteration with restarts (equally weighted to 1) at 10k, 20k, and 40k iterations. The initial learning rate is 10^{-4} , with a minimum value of 10^{-7} .

4. RESULTS

4.1. Metrics

To evaluate the performances of our method, we employ the Structural Similarity Index (SSIM), a well-known metric for quantifying the resemblance between two images. We also adopt the Normalized Mean Squared Error (NMSE), defined as the MSE between \mathbf{I}_{HR} and $\hat{\mathbf{I}}_{\text{HR}}$, normalized by the average of \mathbf{I}_{HR} ². We report this value in dB for convenience. A good result is the one with high SSIM and/or low NMSE. We compute these metrics for every analyzed patch and report the average on the test set.

4.2. Preliminary Studies

We compare the performance of the networks for a single scale factor $\alpha = 4$ and two different data transformations (i.e., \mathcal{T}_S or \mathcal{T}_Q). Fig. 2 summarizes the results in terms of SSIM. We can notice a fairly high quality on all the architectures except for the SRCNN, with a significant boost on attention-based networks (i.e., SANSISR and RCAN). It is worth noticing that \mathcal{T}_Q preprocessing almost always reports better reconstruction results than \mathcal{T}_S strategy. Given these reasons, we

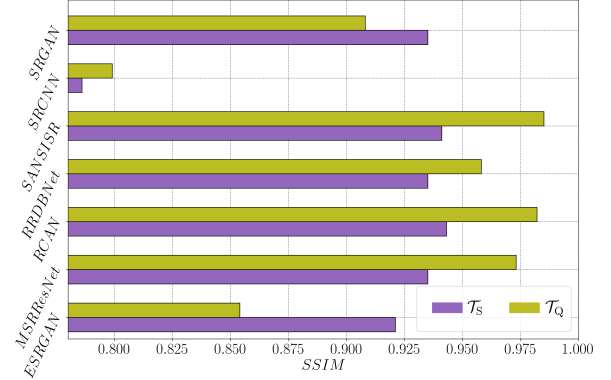


Fig. 2: SSIM achieved by the different networks, for \mathcal{T}_S and \mathcal{T}_Q data transformations.

adopt \mathcal{T}_Q preprocessing in all the remaining experiments. In Fig. 3, we report an example of super-resolved emission maps from the best performing networks.

Fig. 4 shows an example of a comparison between the original and the estimated super-resolved emission map distribution. It is worth noticing that the two distributions present similar behavior. This result is relevant, considering the physical significance of BVOC emission maps. Obtaining a final distribution that matches the original is paramount to preserving the physical meaning of the estimated emission values.

4.3. Solving a Realistic Scenario

In this section, we investigate the performance of our method over more realistic and challenging scenarios. In particular, we aim at performing SR of emission profiles that are not in the same time range and are also in different geographical areas than those used in the training phase.

In a real-world context, the possibility to train with past data and test on future data would be highly desirable. Moreover, the availability of training data inherent to the same geographic area may be infeasible. As mentioned previously, measurements of biogenic emissions are often limited to restricted geographical areas.

To address these scenarios, from the main dataset \mathcal{D} we build two subsets:

- \mathcal{D}_T — *Time*: we consider patches from years 2000-2014 for training, from years 2014-2018 for validation, and from years 2018-2020 for testing. This prevents the network from learning inter-annual biases and enables to investigate the temporal dependence.
- \mathcal{D}_{TA} — *Time & Area*: a split version of \mathcal{D}_T dataset that considers a portion of the spatial coverage for training and the remaining part for testing. This enables us to investigate spatial dependence.

We compare the performances of our method over \mathcal{D}_T and \mathcal{D}_{TA} with those achieved on the initial dataset \mathcal{D} . Notice that \mathcal{D}_{TA} contains the smallest amount of emission pairs due to temporal and geographical constraints. To fairly compare the three scenarios, we randomly sample the bigger datasets \mathcal{D}_T and \mathcal{D} such to have the same cardinality of \mathcal{D}_{TA} . For simplicity, we compare only the three best performing networks namely SANSISR, RCAN and MSRResNet.

Results are shown in Table 1. The three networks perform very similarly, with SANSISR achieving the best results in most cases. It is worth noticing that we can super-resolve unseen emissions from different years (i.e., \mathcal{D}_T results). On the contrary, the performance drops drastically when dealing with geographical areas unseen in the

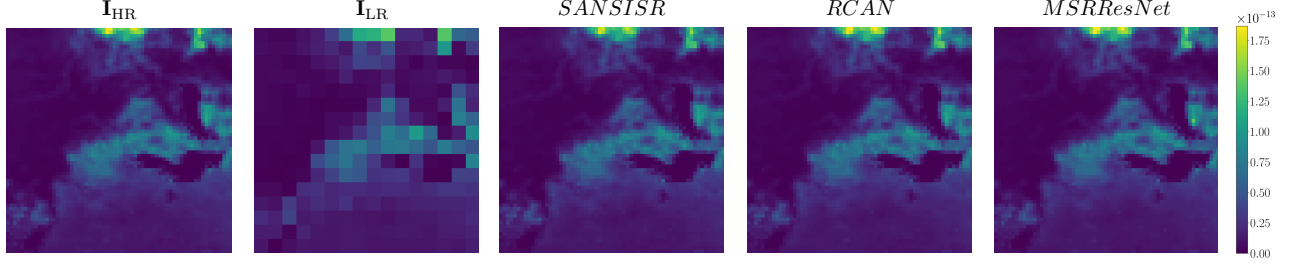


Fig. 3: SISR examples of a generic BVOC emission map from different algorithms. From left to right, the ground truth HR image, the input LR image, and three super-resolved results.

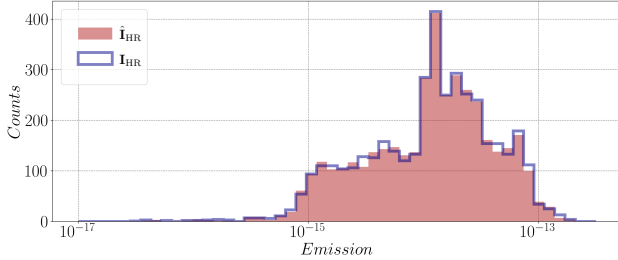


Fig. 4: Distribution of the original HR emission map and of the super-resolved map obtained from the SANSISR network.

Table 1: Performance results over the datasets \mathcal{D} , \mathcal{D}_T and \mathcal{D}_{TA} .

| Dataset | SANSISR | RCAN | MSRResNet |
|--------------------|------------------|------------------|------------------|
| | SSIM / NMSE [dB] | SSIM / NMSE [dB] | SSIM / NMSE [dB] |
| \mathcal{D} | 0.984 / -19.35 | 0.982 / -19.26 | 0.970 / -17.27 |
| \mathcal{D}_T | 0.986 / -21.50 | 0.985 / -20.44 | 0.973 / -17.66 |
| \mathcal{D}_{TA} | 0.769 / -7.31 | 0.774 / -7.32 | 0.788 / -7.26 |

training phase (i.e., \mathcal{D}_{TA} results). This worse result occurs because of the close link between biogenic emissions and land morphology and the vegetation type of the area used in training.

4.4. Towards Generalization in Emissions Super-Resolution

In this section, we address two relevant problems related to the application of SR methods on BVOC emission maps. In particular, we investigate the scale-invariance and the estimation of different compounds. We only show results related to SANSISR architecture, being it the best performing one among the employed networks.

Scale-invariance. This property concerns the ability to generalize SR to data with a spatial resolution not present in training. This could be a useful feature of SR algorithms embedded in the climate modeling frameworks. For instance, if we train the network to pass from $1.00^\circ \times 1.00^\circ$ to $0.25^\circ \times 0.25^\circ$ spatial resolution (i.e., with a $\alpha = 4$ scale factor), we aim at testing the network capabilities in super-resolving emissions from $2.00^\circ \times 2.00^\circ$ to $0.50^\circ \times 0.50^\circ$ (i.e., the scale factor remains the same but the resolution changes).

We investigate the scale-invariance in super-resolving emissions at two scale factors, i.e., $\alpha = 2$ and $\alpha = 4$. Table 2(a) reports the experimental results. As expected, we achieved excellent performance testing data with the same spatial resolution used in training. Whereas, for both $\alpha = 2$ and $\alpha = 4$ scale factors, testing over unseen resolutions leads to significant drops in performance. This indicates that scale-invariance hypotheses are not fully satisfied.

Estimation of different compounds. We investigate the SR of emission maps utilizing compounds different than those adopted in

Table 2: Results for the scale-invariance (a) and for the estimation of different compounds (b). The configuration used during the training phase is reported in bold.

| Scale Factor | Spatial Resolution | (a) | | (b) |
|--------------|---|------------------|----------------------------|----------------|
| | | SSIM / NMSE [dB] | Biogenic Species | |
| $\alpha = 2$ | $0.50^\circ \rightarrow 0.25^\circ$ | 0.993 / -25.58 | \mathcal{D} | 0.985 / -20.87 |
| | $1.00^\circ \rightarrow 0.50^\circ$ | 0.834 / -8.41 | \mathcal{D}_{mon} | 0.875 / -15.76 |
| | $2.00^\circ \rightarrow 1.00^\circ$ | 0.659 / -5.24 | \mathcal{D}_{met} | 0.752 / -13.30 |
| $\alpha = 4$ | $1.00^\circ \rightarrow 0.25^\circ$ | 0.985 / -20.86 | \mathcal{D}_{ses} | 0.905 / -16.03 |
| | $2.00^\circ \rightarrow 0.50^\circ$ | 0.603 / -4.84 | | |

training. As the scale-invariance, this property could be a desirable feature in atmospheric modeling frameworks for enhancing the resolution of a generic chemical compound.

We build three datasets similar to \mathcal{D} but containing emissions of diverse compounds. We select monoterpenes (\mathcal{D}_{mon}), methanol (\mathcal{D}_{met}), and sesquiterpenes (\mathcal{D}_{ses}), since these are the most responsible compounds for the majority of the global BVOC emission [4]. We train our method over the reference dataset \mathcal{D} and test on the three datasets. Results are depicted in Table 2(b). Given the similarity of their chemical structure with that of isoprene [30], it is worth noticing that terpenoids like monoterpenes (i.e., \mathcal{D}_{mon}) and sesquiterpenes (i.e., \mathcal{D}_{ses}) could be used as input to our algorithm, with results that are still acceptable if we consider the benefits that SR emission maps could give to air quality and climate models.

5. CONCLUSIONS

This work focused on enhancing the spatial resolution of BVOC emission maps using DL techniques, proposing a suitable data pre-processing. Super-resolution of BVOC emission maps is critical since global inventories of BVOC measurements are currently unavailable to the modeling communities, and processing existing emissions appears to be the only way to produce maps with high spatial resolution. The overall high performance of the proposed method shows that we effectively generalize to unseen data, achieving accurate estimations of potential future BVOC emissions. We also indicate possible avenues towards generalization of SR algorithms, investigating the scale-invariance and testing different compounds. In the future, we will extend our work through the use of Physics-Informed Neural Networks (PINN), considering both data and the physics behind the process. Super-resolved BVOC emissions could represent an invaluable source for air quality and climate products, allowing to better explain how these compounds affect humans and global climate change.

6. REFERENCES

- [1] M. Cai, C. An, and C. Guy, “A scientometric analysis and review of biogenic volatile organic compound emissions: Research hotspots, new frontiers, and environmental implications,” *Renewable and Sustainable Energy Reviews*, vol. 149, pp. 1–15, 2021.
- [2] A. B. Guenther, X. Jiang, C. L. Heald, *et al.*, “The Model of Emissions of Gases and Aerosols from Nature version 2.1 (MEGAN2.1): An extended and updated framework for modeling biogenic emissions,” *Geoscientific Model Development*, vol. 5, pp. 1471–1492, 2012.
- [3] A. Guenther, C. N. Hewitt, D. Erickson, *et al.*, “A global model of natural volatile organic compound emissions,” *Journal of Geophysical Research*, vol. 100, p. 8873, 1995.
- [4] K. Sindelarova, J. Markova, D. Simpson, *et al.*, “High-resolution biogenic global emission inventory for the time period 2000–2019 for air quality modelling,” *Earth System Science Data*, vol. 14, pp. 251–270, 2022.
- [5] C. Calfapietra, S. Fares, F. Manes, *et al.*, “Role of Biogenic Volatile Organic Compounds (BVOC) emitted by urban trees on ozone concentration in cities: A review,” *Environmental Pollution*, vol. 183, pp. 71–80, 2013.
- [6] B. Opacka, J.-F. Müller, T. Stavrakou, *et al.*, “Global and regional impacts of land cover changes on isoprene emissions derived from spaceborne data and the MEGAN model,” preprint, 2021.
- [7] C. N. Hewitt, B. Langford, M. Possell, *et al.*, “Quantification of VOC emission rates from the biosphere,” *TrAC Trends in Analytical Chemistry*, vol. 30, pp. 937–944, 2011.
- [8] D. M. Lawrence, R. A. Fisher, C. D. Koven, *et al.*, “The Community Land Model Version 5: Description of New Features, Benchmarking, and Impact of Forcing Uncertainty,” *Journal of Advances in Modeling Earth Systems*, vol. 11, pp. 4245–4287, 2019.
- [9] X. Gao, K. Zhang, D. Tao, and X. Li, “Image super-resolution with sparse neighbor embedding,” *IEEE Transactions on Image Processing*, vol. 21, no. 7, pp. 3194–3205, 2012.
- [10] S. Dai, M. Han, W. Xu, *et al.*, “Softcuts: A soft edge smoothness prior for color image super-resolution,” *IEEE Transactions on Image Processing (TIP)*, vol. 18, no. 5, pp. 969–981, 2009.
- [11] C. Dong, C. C. Loy, K. He, and X. Tang, “Learning a Deep Convolutional Network for Image Super-Resolution,” in *European Conference on Computer Vision (ECCV)*, 2014.
- [12] Y. Liu, Y. Qiao, Y. Hao, *et al.*, “Single Image Super Resolution Techniques Based on Deep Learning: Status, Applications and Future Directions,” *Journal of Image and Graphics*, vol. 9, pp. 74–86, 2021.
- [13] F. Salvetti, V. Mazzia, A. Khaliq, and M. Chiaberge, “Multi-Image Super Resolution of Remotely Sensed Images Using Residual Attention Deep Neural Networks,” *Remote Sensing*, vol. 12, p. 2207, 2020.
- [14] B. M. Nguyen, G. Tian, M.-T. Vo, *et al.*, “Convolutional neural network modelling for modis land surface temperature super-resolution,” in *European Signal Processing Conference (EUSIPCO)*, 2022, pp. 1806–1810.
- [15] T. Izumi, M. Amagasaki, K. Ishida, and M. Kiyama, “Super-resolution of sea surface temperature with cnn and gan-based methods,” *Journal of Water and Climate Change*, vol. 13, pp. 1673–1683, 2022.
- [16] D. T. Lloyd, A. Abela, R. A. Farrugia, *et al.*, “Optically Enhanced Super-Resolution of Sea Surface Temperature Using Deep Learning,” *IEEE Transactions on Geoscience and Remote Sensing*, vol. 60, pp. 1–14, 2022.
- [17] R. Brecht, L. Bakels, A. Bihlo, and A. Stohl, “Improving trajectory calculations by FLEXPART 10.4+ using deep learning inspired single image superresolution,” *EGUphere*, vol. 2022, pp. 1–17, 2022.
- [18] A. Tani and T. Mochizuki, “Review: Exchanges of volatile organic compounds between terrestrial ecosystems and the atmosphere,” *Journal of Agricultural Meteorology*, vol. 77, no. 1, pp. 66–80, 2021.
- [19] F. Loreto and J.-P. Schnitzler, “Abiotic stresses and induced bvocs,” *Trends in Plant Science*, vol. 15, no. 3, pp. 154–166, 2010.
- [20] J. Feldner, M. O. P. Ramacher, M. Karl, *et al.*, “Analysis of the effect of abiotic stressors on BVOC emissions from urban green infrastructure in northern Germany,” *Environmental Science: Atmospheres*, vol. 2, no. 5, pp. 1132–1151, 2022.
- [21] M. Ma, Y. Gao, A. Ding, *et al.*, “Development and Assessment of a High-Resolution Biogenic Emission Inventory from Urban Green Spaces in China,” *Environmental Science & Technology*, vol. 56, no. 1, pp. 175–184, 2022.
- [22] F. Pedregosa, G. Varoquaux, A. Gramfort, *et al.*, “Scikit-learn: Machine learning in Python,” *Journal of Machine Learning Research*, vol. 12, pp. 2825–2830, 2011.
- [23] C. Ledig, L. Theis, F. Huszar, *et al.*, “Photo-Realistic Single Image Super-Resolution Using a Generative Adversarial Network,” in *IEEE Conference on Computer Vision and Pattern Recognition (CVPR)*, 2017.
- [24] Y. Zhang, K. Li, K. Li, *et al.*, “Image Super-Resolution Using Very Deep Residual Channel Attention Networks,” in *European Conference on Computer Vision (ECCV)*, 2018.
- [25] X. Wang, K. Yu, S. Wu, *et al.*, “ESRGAN: Enhanced Super-Resolution Generative Adversarial Networks,” in *European Conference on Computer Vision (ECCV)*, 2019.
- [26] T. Dai, J. Cai, Y. Zhang, *et al.*, “Second-Order Attention Network for Single Image Super-Resolution,” in *IEEE Conference on Computer Vision and Pattern Recognition (CVPR)*, 2019.
- [27] K. Zhang, S. Gu, R. Timofte, *et al.*, “AIM 2019 Challenge on Constrained Super-Resolution: Methods and Results,” in *arXiv*, 2019.
- [28] I. Loshchilov and F. Hutter, “SGDR: Stochastic gradient descent with warm restarts,” in *International Conference on Learning Representations (ICLR)*, 2017.
- [29] ———, “Decoupled Weight Decay Regularization,” in *International Conference on Learning Representations (ICLR)*, 2019.
- [30] V. Ninkuu, L. Zhang, J. Yan, *et al.*, “Biochemistry of Terpenes and Recent Advances in Plant Protection,” in *International Journal of Molecular Sciences*, vol. 22, no. 11, p. 5710, 2021.